2.3. SLIDING MODE BASED OUTER CONTROL LOOP FOR INDUCTION MOTOR DRIVES WITH FORCED DYNAMICS

***Abstract*:** Through the load torque estimation, the basic FDC based IM drive control system presented in the last two sections offers higher robustness with respect to parameter uncertainties and external load torques than conventional shaft sensorless speed control methods, due to the use of the load torque estimate in the control law, as explained in previous sections. There is still, however, room for improvement when compared with the performance of some drives employing shaft sensors. To achieve a closer approach to this performance, a scheme is presented using the sliding mode control principle. It will be recalled that the basic FDC system has a cascade control structure consisting of an inner loop, which is a stator current control loop, and a shaft sensorless FDC based speed control loop, enabling a user specified dynamic performance to be obtained according to dynamic modes such as presented and described in Chapter 1. This speed control loop will now be referred to as the middle loop, since the robustness enhancement will be produced by the addition of an outer sliding mode control loop. Simulation and experimental results show good correspondence with the theoretical predictions and demonstrate the intended robustness improvements.

2.3.1 Introduction

The new FDC based IM drive control system already presented based on feedback linearisation [1], principles of vector control [2] and sliding mode control (SMC) [3] will be operated in the *first order linear dynamic mode* for this robustness enhancement investigation. As stated previously, the system operates without shaft sensors, only the stator currents being measured and the applied stator voltages being determined by the computed switching algorithm of the inverter with a knowledge of the instantaneous DC link voltage. The rotor magnetic flux norm dynamics is also chosen as linear and of first order, as described in section 2.1.2.

Forced dynamic control is applicable in many non-linear multivariable automatic control applications and was originally developed for electrical drives employing IM [4] and experimentally verified in [5]. Various forced dynamics for IM drives, including constant torque demand, second order speed dynamics, and the possibility of directly controlling the drive acceleration, were introduced in [6] and verified by simulations. The experimental results for all these three prescribed dynamics were presented in [7]. Such a control system is suitable for sensorless control of electric drives employing IM with moderate accuracy ($\cong 5\%$). The original basic sensorless IM drive control system with forced dynamics is shown in Fig. 2.3.1. It contains a set of three observers for estimation of the rotor magnetic flux, the rotor angular speed and the load torque.

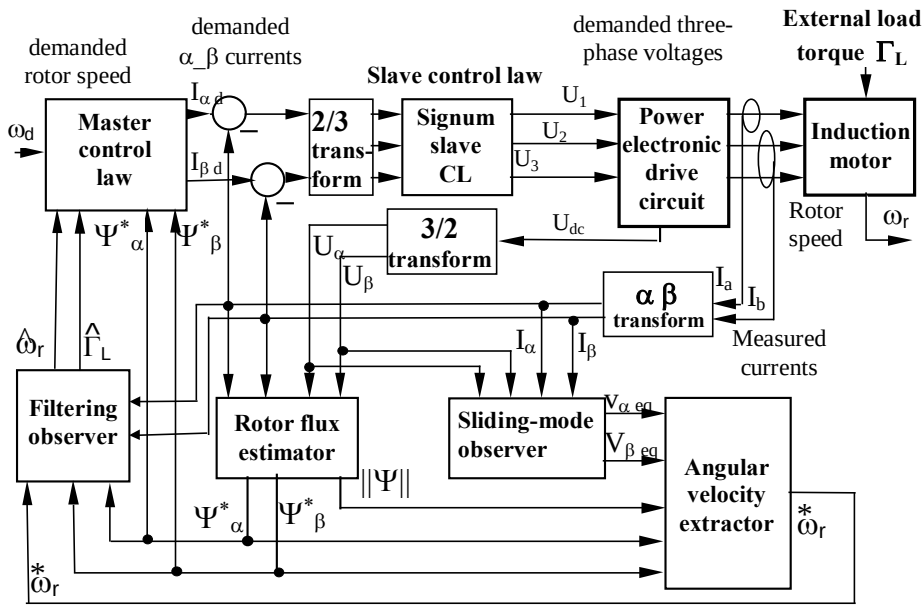

Fig. 2.3.1 Original control system of shaft sensorless speed controlled electric drive with IM and forced dynamic

Since the control law itself, the magnetic flux observer, the rotor angular speed observer and load torque observer are all model-based, i.e., dependent on estimates of the motor parameters, then some sensitivity to the errors in these estimates is expected. It means that the closed-loop performance of the whole control system is

a affected by errors in the estimates. To reduce this sensitivity the intention here is to close an outer control loop around the original close-loop system and to improve the robustness of the whole control system. Model reference adaptive control (MRAC) and SMC based outer control loops were theoretically suggested in [8]. The first experimental results for the MRAC outer loop were reported in [9]. The purpose of this chapter is the experimental verification of the SMC based outer control loop. A schematic block diagram of the overall control system, including the SMC outer control loop, is shown in Fig. 2.3.2.

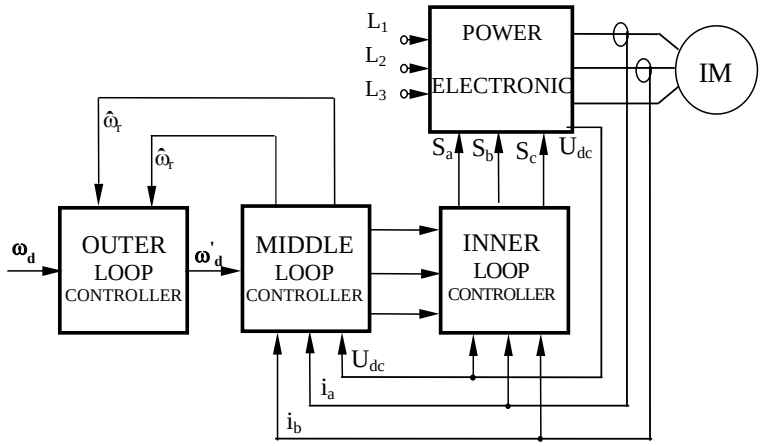

Fig. 2.3.2 Modified forced dynamic drive control system with the SMC outer loop

Thus, the original FDC based speed controller becomes the *middle loop controller* of the new scheme.

2.3.2 Control System

2a) Model of Motor and Load

The α, β frame based model of IM in matrix notation is as follows:

$$\dot{\omega}_r = \frac{1}{J}(\Gamma - \Gamma_L) = \frac{1}{J}\left(c_5 \boldsymbol{\Psi}^T \mathbf{T}^T \mathbf{I} - \Gamma_L\right) \tag{2.3.1}$$

$$\dot{\boldsymbol{\Psi}} = -\mathbf{P}(\omega_r)\boldsymbol{\Psi} + c_4 \mathbf{I} \tag{2.3.2}$$

$$\dot{\mathbf{I}} = c_1\left[c_2 \mathbf{P}(\omega_r)\boldsymbol{\Psi} - a_1 \mathbf{I} + \mathbf{U}\right], \tag{2.3.3}$$

where $\mathbf{\Psi}^T = [\Psi_\alpha \ \Psi_\beta]$, $\mathbf{I}^T = [\imath_\alpha \ \imath_\beta]$, $\mathbf{U}^T = [u_\alpha \ u_\beta]$, and $c_1 = L_r/(L_s L_r - L^2_m)$, $c_2 = L_m/L_r$, $c_3 = R_r/L_r = 1/T_r$, $c_4 = L_m/T_r$, $c_5 = 1{,}5.p.L_m/L_r$ and $a_1 = R_s + (L^2_m/L^2_r)R_r$. Also:

$$\mathbf{P}(\omega_r) = \begin{bmatrix} c_3 & p\omega_r \\ -p\omega_r & c_3 \end{bmatrix} \qquad \text{and} \qquad T = \begin{bmatrix} 0 & -1 \\ 1 & 0 \end{bmatrix}. \tag{2.3.4}$$

2b) The Middle Loop Controller

2b1) The forced dynamic control law

On the basis that the inner loop controller maintains zero stator current errors, equation (2.3.3) is eliminated from the control problem. The feedback linearisation principles [1] are used for the forced dynamic control law development. The linearising functions, which force the system variables to obey specified linear closed-loop differential equations, are formulated for the rotor speed and the magnetic flux norm. In this application, they are first order with time constants T_ω for the rotor speed and T_Ψ for the demanded rotor flux norm. These two variables therefore satisfy equations:

$$\dot{\omega}_r = \frac{1}{T_\omega}(\omega_d - \omega_r) \tag{2.3.5a}$$

$$\| \dot{\Psi} \| = \frac{1}{T_\Psi}(\| \Psi \|_d - \| \Psi \|), \tag{2.3.5b}$$

where $\| \Psi \| = \Psi_\alpha^2 + \Psi_\beta^2$.

The linearising function for $\dot{\omega}_r$ is then obtained by equating the right hand sides of equations (2.3.1) and (2.3.5a):

$$\mathbf{\Psi}^T \mathbf{T}^T \mathbf{I} = \frac{1}{c_5}\left[\frac{J}{T_\omega}(\omega_d - \omega_r) + \Gamma_L \right]. \tag{2.3.6}$$

The derivative of the rotor magnetic flux norm can be proven to be given by (2.3.7a) and equating the right hand sides of equations (2.3.5b) and (2.3.7a) yields (2.3.7b):

$$\| \dot{\Psi} \| = -2(c_3 \| \Psi \| - c_4 \mathbf{\Psi}^T * \mathbf{I}) \tag{2.3.7a}$$

$$\boldsymbol{\Psi}^{T}\mathbf{I}=\frac{c_3}{c_4}\|\Psi\|+\frac{1}{2c_4T_\Psi}\left(\|\Psi\|_d-\|\Psi\|\right). \tag{2.3.7b}$$

The required control law is then obtained by combining equations (2.3.6) and (2.3.7b), but first, the state variables (x) are replaced by their estimates ($\hat{x}$) from the observers. Also, the constant motor parameters (p) are replaced by their estimates $(\tilde{p})$. Furthermore, the fictitious control vector, **I**, is replaced by the demanded current vector, $\mathbf{I_d}$, which is the inner control loop reference input. Thus, the forced dynamic control law is:

$$\mathbf{I_d}=\frac{1}{\|\Psi^*\|}\begin{bmatrix}-\Psi_\beta^* & \Psi_\alpha^*\\ \Psi_\alpha^* & \Psi_\beta^*\end{bmatrix}\begin{bmatrix}\dfrac{1}{\tilde{c}_5}\left(\dfrac{\tilde{J}}{T_\omega}\left(\omega_d-\hat{\omega}_r\right)+\hat{\Gamma}_L\right)\\ \dfrac{\tilde{c}_3}{\tilde{c}_4}\|\Psi^*\|+\dfrac{1}{2\tilde{c}_4T_\Psi}\left(\|\Psi^*\|_d-\|\Psi^*\|\right)\end{bmatrix}. \tag{2.3.8}$$

It should be noted that the constant external disturbance torque, Γ_L , is treated as a state variable and estimated in the observer together with the other state variables. The nominal closed-loop system is then governed by the transfer function:

$$\frac{\omega_r(s)}{\omega_d(s)}=\frac{1}{1+sT_\omega}. \tag{2.3.9}$$

This feature a) automatically yields soft starting and b) renders the system ideally suited for inclusion as an *adjustable* linear element in an overall control system such as in motion control, where an outer linear position control loop would be added.

2c) State Estimation

Detailed description of this part was already given as section 2.1.3 and in abbreviated form as section 2.2.3 and reader is referred for study of state estimation and observers design to the corresponding sections for this.

2.3.3 Sliding Mode Outer Loop Controller

Sliding mode based control law. Sliding mode control [3] is a form of bang-bang control in which the plant state is forced towards and maintained within a close vicinity of a boundary determined by the control system designer. If, for a single input, single output plant, the state variables are chosen as the controlled output and its derivatives up to an order equal to '*r-1*', where '*r*' is the plant rank, then if the state is maintained precisely on the boundary, the closed loop dynamics is determined by the boundary alone and is *independent of the plant parameters and any external disturbances*. The state point then appears to *slide* in the boundary. Hence the term *sliding motion* is used. Since the boundary is an '*r-1*' dimensional hyper-surface in an '*r*' dimensional output derivative space, the order of the closed-loop system in the sliding mode is always '*r-1*'. This fact is made use of in the outer loop controller.

Consider now the closed-loop system created by the inner and middle control loops. This will have the nominal transfer function:

$$\frac{\hat{\omega}_r(s)}{\omega_d(s)} = \frac{1}{1+sT_\omega}. \tag{2.3.10}$$

Since the IM is inherently nonlinear, errors introduced by uncertainties of its parameter values will cause the linear dynamics of (2.3.10) to become nonlinear. It may be shown that the sliding mode outer loop can compensate for this, but to illustrate its action more simply, these parametric uncertainties, external load torque and imperfect operation of the middle control loop due to the non-zero iteration interval will (roughly) be represented by a change of time constant and DC gain. Then the combined inner and middle loop dynamics resulting from the aforementioned errors and disturbances may be represented by the transfer function:

$$\frac{\hat{\omega}_r(s)}{\omega_d(s)} = \frac{K_d}{1+sT_\omega^{'}}, \tag{2.3.11}$$

where $K_d > 0 \;\&\; \neq 1$ and $T_\omega^{'} > 0 \;\&\; \neq T_\omega$.

In order to create a sliding mode control loop that does not reduce the system

order (equal to the rank without transfer function zeros), which is required to yield the closed-loop system dynamics of (2.3.10), a pure integrator is introduced at the speed reference input of the middle control loop to increase its order by one before formation of the sliding mode outer loop. Fig. 2.3.3 shows this, treated as a new plant with control variable, u', and with the outer loop controller.

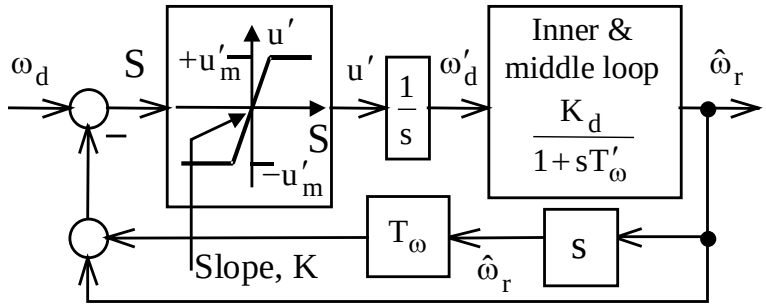

Fig. 2.3.3 Sliding mode based outer control loop

The output derivative, $\dot{\hat{\omega}}_r$, may be obtained without differentiation by using the second of the filtering observer equations. If the gain, K, is infinite, then the transfer characteristic between S and u' yields the bang-bang control law used in classical sliding mode control:

$$u' = u'_m \, \mathrm{sgn}(S), \tag{2.3.12}$$

where:

$$S = \omega_d - \hat{\omega}_r - T_\omega \dot{\hat{\omega}}_r . \tag{2.3.13}$$

The operation of such a control loop may be examined in the phase-plane, i.e, the graph of $\dot{\hat{\omega}}_r$ against $\hat{\omega}_r$. The control, u', switches between $+u_m$ and $-u_m$, when $S = 0$. Setting this condition in (2.3.13) then yields the *switching boundary*. This is shown in Fig. 2.3.4 together with a family of state trajectories commencing from different starting points (referred to as a *phase portrait*).

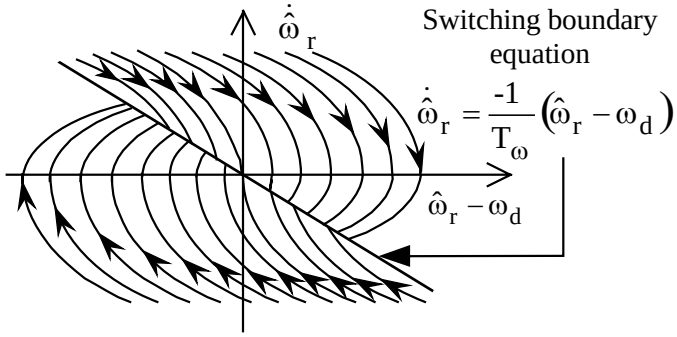

Fig. 2.3.4 Closed-loop phase portrait and switching boundary for sliding mode based outer control loop

It is evident that over most of the boundary shown, the *trajectories of the phase portrait are directed towards the boundary from both sides*, meaning that once the boundary is reached, the trajectory is maintained close to it while the control, u', rapidly switches (*control chatter*). This is the condition for sliding motion and the controller described is the classical sliding mode controller. Under these circumstances, the closed-loop system obeys the switching boundary equation shown in Fig. 2.3.4 and this corresponds to transfer function (2.3.11) with K_d=1 and $T'_\omega = T_\omega$, e. i.

$$\frac{\hat{\omega}_r(s)}{\omega_d(s)} = \frac{1}{1+sT_\omega}. \qquad (2.3.14)$$

This means that without parameter uncertainties or external load torque, the outer loop controller makes no difference to the closed-loop dynamics. It merely compensates for the effects of the parameter mismatches and load torque, thereby yielding the required robustness. It is important to note, however, that with this shaft sensorless system, the control can only be as accurate as the *speed estimate*, $\hat{\omega}_r$.

In the final control system design, the control chatter, which would interact in an undesirable way with the switching of the power electronics, is eliminated by reducing the slope, K, in Fig. 2.3.3 to a finite, but relatively large value. Then it may be shown that as $K \to \infty$, $S \to 0$, and therefore the resulting performance is similar to the classical sliding mode controller, yielding similar robustness provided $|u'|<u'_m$.

Since an angular acceleration estimate from filtering observer would be likely to contain substantial noise contamination, an opportunity to use an equivalent outer loop control algorithm avoiding this was taken (*although this is available from the filtering observer*). With reference to Figure 2.3.3, the integrator effectively cancels the differentiator in the inner feedback loop. The resulting block diagram is shown in Fig. 2.3.5 and this yields the SMC based control algorithm of equation (2.3.15).

$$\omega'_d = K_{SM}\left[\int(\omega_d - \hat{\omega}_r)dt - T_\omega \hat{\omega}_r\right] \quad . \tag{2.3.15}$$

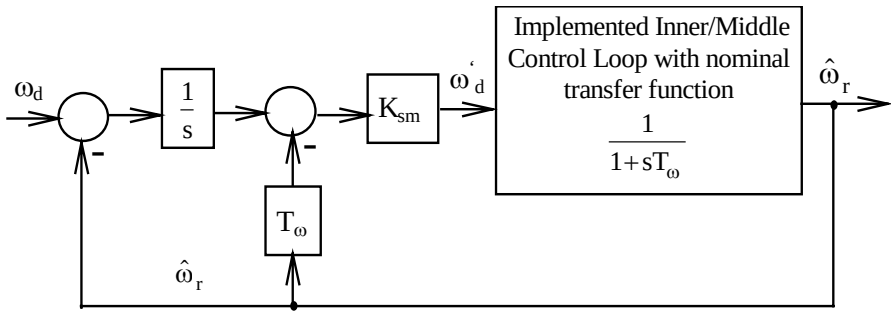

Fig. 2.3.5 SMC based outer control loop implemented in experiments

2.3.4 Simulation and Experimental Results

The following set of simulations and experiments demonstrate the performance of the control system by simultaneously applying i) a step angular velocity demand of ω_d=100 rad/s, with time constant T_ω=0,2 s, ii) a step rotor magnetic flux norm demand of $\|\Psi_d\|$=5e-3 $(Vs)^2$, with prescribed time constant T_Ψ=2,5 ms and with zero initial state variables throughout the system. The simulations were carried out in the Matlab environment, the differential equations of the motor and observers being integrated using the explicit Euler method. The simulations presented include the achieved sampling interval and the finite word length used in the experiments. The parameters of the induction motor relevant to both the simulations and the experiments are listed in the Appendix.

For the experiments, the control algorithms were implemented on a PC equipped with a PC Lab card. The stator currents were measured through '*LEM*'

current transformers and evaluated using a '*PC Lab Card PL812'*. A six-transistor ***Semikron*** IGBT module was used as the three-phase inverter. All the experiments presented were carried out with a DC supply voltage of U_{DC}=60 V and a step rotor speed demand of ω_{dem}=100 rad/s and a time constant of T_{ω}=0,2 s. Data logging of the experimental variables was carried out for a 1,82 s time interval. The eddy current brake served as a load during the experiments.

In all the graphs presented, the stator current and rotor magnetic flux components as functions of time during the starting interval $t \in$(0-0,1) s are shown in subplots (a). The estimates of the rotor speed from the pseudo-sliding mode observer are shown in subplots (b) as functions of time for the whole data logging interval. Plots (c) show the load torque estimate, $\hat{\Gamma}_L$, from the filtering observer together with the rotor magnetic flux norm estimate $\|\Psi\|$. Finally, subplots (d) show the ideal rotor speed, ω_{id}, together with real rotor speed, ω_r, and its estimate, $\hat{\omega}_r$, from filtering observer for the whole data logging interval. The simulation and experimental results are plotted, respectively, in the left and right columns.

The simulation and experimental results obtained with the middle and inner control loops, excluding the SMC outer loop, are shown in Fig. 2.3.6. The errors between the ideal rotor speed and the real and estimated rotor speeds can be clearly seen in subplots (d). These errors, which are attributed to imperfections in the constant parameter estimates, and the finite gains of the observers imposed by the non-zero sampling interval, persist even in the steady-state.

The simulation and experimental results corresponding to those of Fig. 2.3.6, but including the SMC outer loop, are shown in Fig. 2.3.7. The significant reduction of the aforementioned errors brought about by the SMC outer control loop, both during the acceleration of the drive and in the steady state, is evident by comparison of these two figures.

The experimental results confirm that the addition of a SMC based outer control loop to the forced dynamic shaft sensorless speed control of electric drives with induction motors considerably improves their performance. The drive follows the ideal speed response much more closely during speed-up and also in the steady-state. Even a substantial increase of the load torque was found not to deteriorate the drive performance significantly after the addition of the SMC outer loop and this improvement is even enhanced at higher rotor speeds.

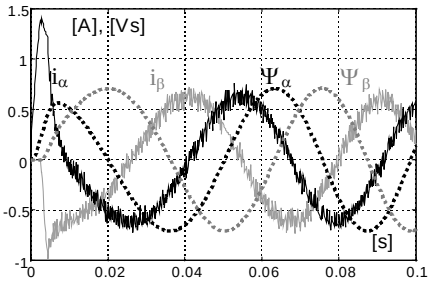

*a1) Stator current and rotor magnetic flux components - **simulation***

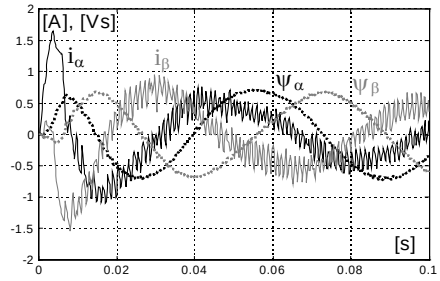

*a2) Stator current and rotor magnetic flux components - **experiment***

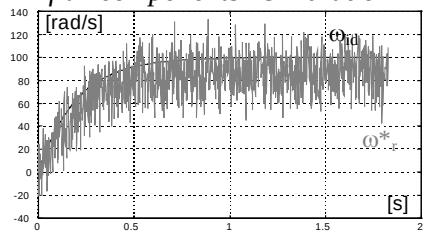

b1) Estimated, unfiltered rotor speed from pseudo-sliding mode observer

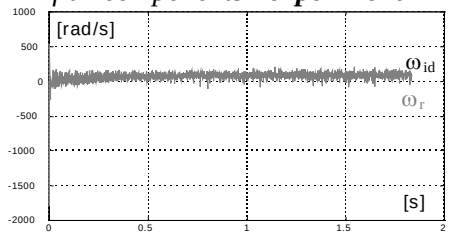

b2) Estimated, unfiltered rotor speed from pseudo-sliding mode observer

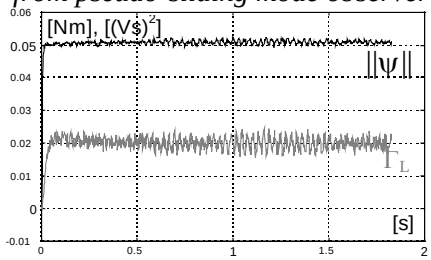

c1) Estimated rotor magn. flux norm and load torque from filtering observer

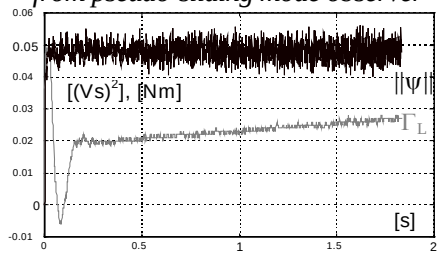

c2) Estimated rotor magn. flux norm and load torque from filtering observer

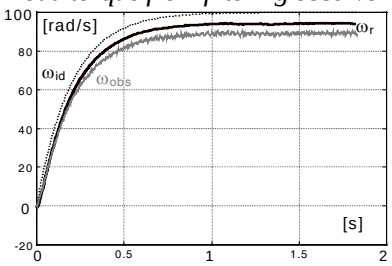

d1) Ideal speed response, real and estimated rotor speed

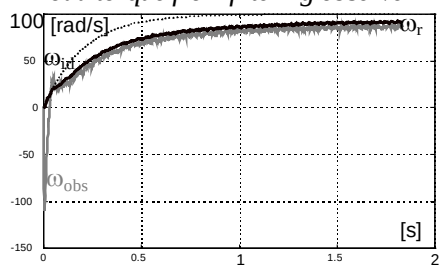

d2) Ideal speed response, real and estimated rotor speed

Fig. 2.3.6 Speed response and corresponding state variables with inner and middle control loops alone

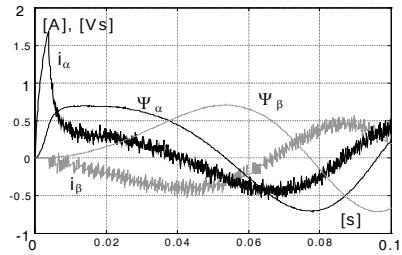

*a1) Stator current and rotor magnetic flux components - **simulation***

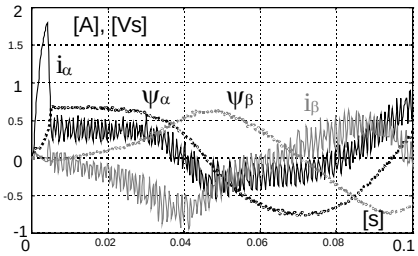

*a2) Stator current and rotor magnetic flux components - **experiment***

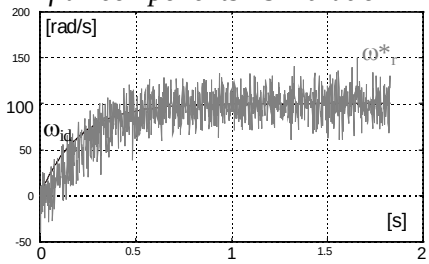

b1) Estimated, unfiltered rotor speed from pseudo-sliding mode observer

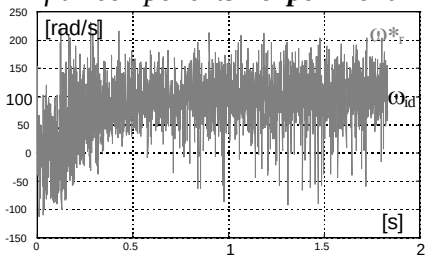

b2) Estimated, unfiltered rotor speed from pseudo-sliding mode observer

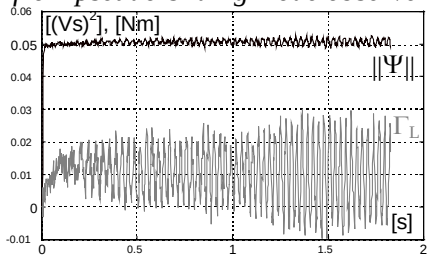

c1) Estimated rotor magn. flux norm and load torque from filtering observer

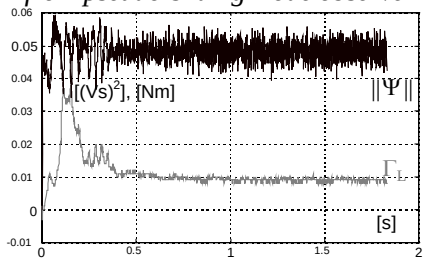

c2) Estimated rotor magn. flux norm and load torque from filtering observer

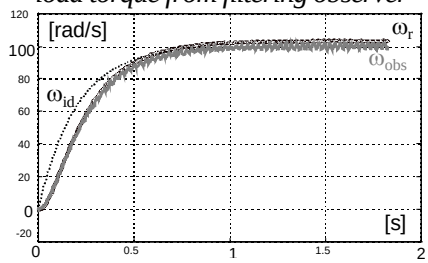

d1) Ideal speed response, real and estimated rotor speed

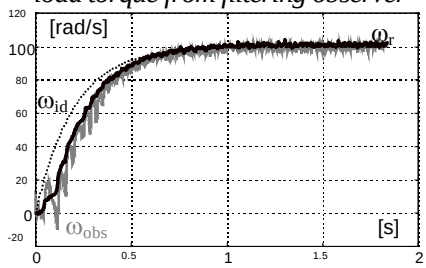

d2) Ideal speed response, real and estimated rotor speed

Fig. 2.3.7 Speed response and corresponding state variables with sliding mode based outer control loop

2.3.5 Conclusions and Recommendations

The preliminary experimental results confirm that the addition of a SMC based outer control loop to the forced dynamic shaft sensorless speed IM drive control system considerably improves its performance. Suggestions for future research work are:

a detailed investigation of robustness with respect to motor and load parameter uncertainties and comparison of the effectiveness of both the MRAC and SMC outer control loops,

implementation of sliding mode based outer control loop for forced dynamic control of synchronous motor electric drives,

a further set of experimental trials for IM drives with higher power ratings together with an investigation of the variation of the filtering observer performance with the pole locations.

2.3.6 References

[1] ISIDORI, A.: '*Nonlinear Control Systems*'. 2nd edition. ***Springer-Verlag*** Berlin, 1990.

[2] BOLDEA, I., NASSAR, A. S.: '*Vector Control of AC Drives*'. ***CRC Press*** London, 1990.

[3] UTKIN, V. I.: '*Sliding Modes in Control and Optimisation*'. ***Springer-Verlag*** Berlin, 1992.

[4] DODDS, S. J., VITTEK, J., UTKIN V. A.: '*Sensorless Induction Motor Drive with Independent Speed and Rotor Magnetic Flux Control - Part I-Theoretical Background and Part II-Simulation and Real Time Implementation*'. **Journal of Electrical Engineering**, Bratislava, vol. 49, y. 1998, No. 7-8 and No. 9-10. pp. 186-193 and pp. 232 - 239.

[5] DODDS, S. J., VITTEK, J., MIENKINA, M.: '*Implementation of a Sensorless Induction Motor Drive Control System with Prescribed Closed-Loop Rotor Magnetic Flux and Speed Dynamics*'. Proceedings of **EPE'97** Conference, *Trondheim, Norway*, Sept. 1997, pp. 4.492 - 4.497.

[6] DODDS, S. J., VITTEK, J., PERRYMAN, R.: '*Forced Dynamic Control of Shaft Sensorless Induction Motor Drive*'. Proceedings of **SPEEDAM'98** Conference, *Sorrento, Italy*, June 1998, pp. A1-9 - A1-14.

[7] VITTEK, J., ALTUS, J., DODDS, S. J., PERRYMAN, R.: '*Induction Motors Electric Drives with Forced Dynamics*'. Proceedings of **IASTED'99** 'Control and Applications' Conference, *Banff, Canada*, July 1999, pp. 177 - 182.

[8] Vittek, J., Dodds S. J.: '*Robust Cascade Forced Dynamic Control of Shaft Sensorless Induction Motor Drives*'. Proceedings of **EDPE'99** Conference, *Stara Lesna, Slovakia*, Oct. 1999, pp. 73 - 79.

[9] VITTEK, J., ALTUS, J., BUDAY, J., MIKLO, J.: *MRAC Improves Performances of Induction Motor Drive with Forced Dynamics*'. Proceedings of **IASTED CA'99** 'Intelligent Control and Systems' Conference, Oct. 1999, *Santa Barbara, CA, USA*, pp. 106 - 116.

Appendix

Three-phase induction motor AM 3~ 4AP80-2 MEZ SIEMENS parameters are as follows:

Induction motor parameters		**Equivalent circuit parameters**	
Rated power	P_n=1.1 kW	Mutual inductance	L_m=0,474 H
Rated speed	ω_n=297.93 rad/s	Stator inductance	L_s=0,482 H
Terminal voltage	Y/Δ 400/230 V	Rotor inductance	L_r=0,482 H
Rated current	Y/Δ 2.4/4.2 A	Stator resistance	R_s=7,15 Ω
Moment of inertia	J=0.035 kgm^2	Rotor resistance	R_r=6,05 Ω

Acknowledgements

The authors wish to thank the **European Commission, Brussels**, for funding the **INCO Copernicus** programme No.960169 **UCODRIVE** and the **Slovak Ministry of Education** for additional financial support of this program by grant No. PL960169.